


Tracking Rydberg atoms with Bose-Einstein condensates

Shiva Kant Tiwari* and Sebastian Wüster†

Department of Physics, Indian Institute of Science Education and Research, Bhopal 462066, India

 (Received 8 October 2018; revised manuscript received 2 February 2019; published 16 April 2019)

We propose to track the position and velocity of mobile Rydberg excited impurity atoms through the elastic interactions of the Rydberg electron with a host condensate. Tracks first occur in the condensate phase, but are then naturally converted to features in the condensate density or momentum distribution. The condensate thus acts analogously to the cloud or bubble chambers in the early days of elementary particle physics. The technique will be useful for exploring Rydberg-Rydberg scattering, rare inelastic processes involving the Rydberg impurities, coherence in Rydberg motion, and forces exerted by the condensate on the impurities. Our simulations show that resolvable tracks can be generated within the immersed Rydberg lifetime and condensate heating is under control. Finally, we demonstrate the utility of this Rydberg tracking technique to study ionizing Rydberg collisions or angular momentum changing interactions with the condensate.

DOI: [10.1103/PhysRevA.99.043616](https://doi.org/10.1103/PhysRevA.99.043616)

I. INTRODUCTION

Tracking particle motion has helped to advance physics for centuries, in developing Newtonian mechanics, understanding Brownian motion, and more recently unraveling the standard model of elementary particle physics. Tracks have allowed the deduction of fundamental theories through studying the deflection of trajectories by conservative and frictional forces. They further indicate decay products and give clues on particle lifetimes via track lengths. Early examples of tracking devices are the bubble chamber [1] and cloud chamber [2], in which an energetic particle leaves an optically visible mark of its passing through interaction with the chamber medium. These devices were later replaced by wire chambers [3] and recently silicon detectors [4].

In ultracold atomic physics, about 25 orders of magnitude below the particle physics energy scales, experiments can dope Bose-Einstein condensates (BECs) with impurities such as ions [5] or Rydberg atoms [6–8]. We show that the phase coherence of the BEC allows its use as a tracking instrument for Rydberg impurities, reminiscent of a bubble chamber in the early days of particle physics. Through elastic collisions of the Rydberg electrons with the condensate atoms, tracks are created in the density of the condensate that record Rydberg trajectories and can be detected by *in situ* measurements [9–11]. Associated phase information also allows one to infer Rydberg velocities and could be read out by interference with a reference condensate [12–16].

Tracking can first verify dipole-dipole and van der Waals (vdW) interactions [17–19] of Rydberg atoms and then explore less-well-studied inelastic reactions that occur when ground-state atoms interact with Rydberg impurities in the ultracold regime [6,7,20]. While such reactions may somewhat limit BECs in tracking other Rydberg dynamics, they

also provide the opportunity to study the timing and evolution during decay processes through the length and features of imprinted tracks.

To demonstrate the feasibility of our ideas, we model up to five Rydberg excited atoms mutually interacting via van der Waals forces while embedded in a BEC. Rydberg atoms move as in Newton's equations, while the BEC evolves according to the Gross-Pitaevskii equation including the effect of the impurity potentials [21–23]. We show that for typical parameters, resolvable phase tracks are obtained within the effective Rydberg lifetime [7] and find that condensate heating during the tracking process is limited. The classical electron probability distribution in a Rydberg state turns out to be a helpful tool for modeling tracking. Finally, we show that the technique can tackle measurements of Rydberg-Rydberg ionization distances and witness angular momentum changing processes under realistic conditions.

This article is organized as follows. We introduce our model of a BEC interacting with Rydberg impurities in Sec. II and discuss the basic effect of phase imprinting [22]. We then show in Sec. III that mobile impurities leave behind plenty of tracking information, in both condensate phase and velocity. These simulations benefited from an approximation based on the classical Rydberg electron probability distribution, which we discuss in Sec. IV. We rule out that excess heating would be problematic for scenarios as discussed in Sec. V and highlight scenarios with detectable slowdown of the impurity by the background condensate in Sec. VI. Applications of Rydberg tracking to the study of exotic atomic physics collisions are suggested in Sec. VII. We summarize in Sec. VIII.

II. INTERACTIONS BETWEEN RYDBERG IMPURITIES AND BECs

Consider a Bose-Einstein condensed gas of N Rb^{87} atoms with mass m mostly in their ground state, among which N_{imp} impurity atoms are excited to a Rydberg state $|\Psi\rangle = |\nu s\rangle$, with principal quantum number $\nu \gg 10$ and $l = 0$ angular

*shiva17@iiserb.ac.in

†sebastian@iiserb.ac.in

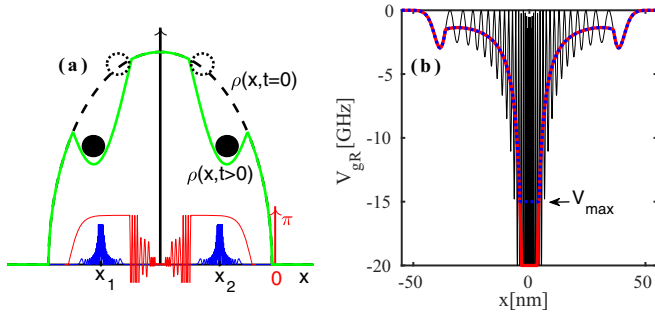


FIG. 1. Sketch showing a one-dimensional cut through a Bose-Einstein condensate that is tracking two repelling Rydberg impurities (black \bullet). (a) Condensate density ρ before (dashed black line) and after (solid green line) Rydberg motion, with corresponding phase signal (oscillating red line) and sketched Rydberg electron wave functions (blue bottom near locations x_1 and x_2). (b) Interaction potential $V_{gR}(\mathbf{R})$ (thin black line) between condensate atoms and a single Rydberg impurity at $x = 0$ for principal quantum number $\nu = 20$. The classical approximation V_c (thick red line) averages over fast oscillations. We also employ the indicated cutoff V_{\max} (dotted blue line).

momentum. This is sketched for $N_{\text{imp}} = 2$ in Fig. 1(a). We denote the location of impurities by \mathbf{x}_n . As discussed in [6,22–25], we can then model the BEC in the presence of Rydberg impurities with the Gross-Pitaevskii equation (GPE)

$$i\hbar \frac{\partial}{\partial t} \phi(\mathbf{R}) = \left(-\frac{\hbar^2}{2m} \nabla^2 + W(\mathbf{R}) + g_{2D} |\phi(\mathbf{R})|^2 + \sum_n^{N_{\text{imp}}} V_0 |\Psi(\mathbf{R} - \mathbf{x}_n)|^2 \right) \phi(\mathbf{R}), \quad (1)$$

where $\phi(\mathbf{R})$ is the condensate wave function and $W(\mathbf{R}) = m\omega_r^2(x^2 + y^2)/2$ describes a two-dimensional (2D) harmonic trap, with $\mathbf{R} = [x, y]^T$. The third dimension is frozen through tight trapping $\omega_z^2 \gg \omega_r$ (see, e.g., [26] and Appendix A), hence $g_{2D} = g_{3D}/\sqrt{2\pi}\sigma_z$ describes the effective strength of atomic collisions, where $g_{3D} = 4\pi\hbar^2 a_s/m$, with atom-atom s -wave scattering length a_s and $\sigma_z = \sqrt{\hbar/m\omega_z}$. To formally justify the simple 2D reduction with respect to the Rydberg-BEC interaction, we require a scenario as shown in Fig. 2,

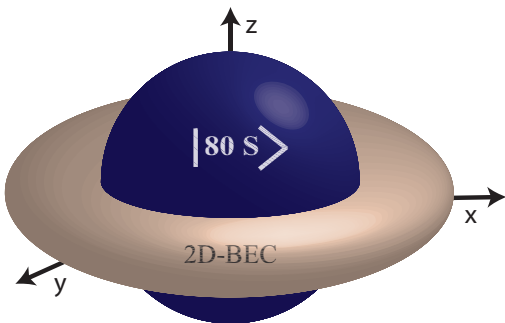


FIG. 2. Sketch of the Rydberg orbital with a larger z extension than the host BEC, justifying the replacement of the BEC-Rydberg interaction by a 2D cut at $z = 0$ through the complete potential.

with the condensate more tightly confined in the z direction than the Rydberg orbital radius.

The last line in (1) represents interactions between the ground-state condensate atoms and impurities due to elastic collisions of the Rydberg electron and condensate atoms [27]. The potential for a single impurity $V_{gR,n}(\mathbf{R}) \equiv V_0 |\Psi(\mathbf{R} - \mathbf{x}_n)|^2$ is sketched in Fig. 1(b). Its strength is set by $V_0 = 2\pi\hbar^2 a_e/m_e$ containing the electron-atom scattering length $a_e = -16.04a_0$, where a_0 is the Bohr radius.¹ The potential shape is set by the Rydberg electron density $|\Psi(\mathbf{R})|^2$, where $\Psi(\mathbf{R}) = \langle \mathbf{R} | \Psi \rangle$.

To describe mobile Rydberg impurities, we couple Eq. (1) to Newton's equations governing their motion

$$m \frac{\partial^2}{\partial t^2} \mathbf{x}_n = -\nabla_{\mathbf{x}_n} [V_{RR}(\mathbf{X}) + \bar{V}(\mathbf{x}_n)], \quad (2)$$

where $V_{RR}(\mathbf{X}) = \sum_{n>m} C_6(\nu)/|\mathbf{x}_n - \mathbf{x}_m|^6$ is the vdW interaction between Rydberg impurities, with dispersion coefficient C_6 taken from [18], and $\mathbf{X} = [\mathbf{x}_1, \dots, \mathbf{x}_{N_{\text{imp}}}]^T$ grouping all impurity positions. In addition, the n th impurity experiences an effective potential $\bar{V}(\mathbf{x}_n) = \int d^2\mathbf{R} V_0 |\Psi(\mathbf{R} - \mathbf{x}_n)|^2 |\phi(\mathbf{R})|^2$ from the backaction of the condensate [21,23,24]. See Appendix A for the 2D reduction.

Let us split the BEC wave function $\phi(\mathbf{R}) = \sqrt{\rho(\mathbf{R})} e^{i\varphi(\mathbf{R})}$ into a real density ρ and phase φ . Then the initial effect of each impurity is to imprint a phase $\varphi \sim -V_{gR,n}(\mathbf{R})\Delta t/\hbar$, within a short time Δt [22,28].

Velocity dependence of phase imprinting

Ignoring all energy contributions except the BEC-impurity interaction, for a single impurity with trajectory $\mathbf{x}(t) = \mathbf{v}t$ the solution of Eq. (1) at time t is given by $\phi(\mathbf{R}, t) = \phi(\mathbf{R}, 0) \exp^{i\varphi(\mathbf{R}, t)}$, where

$$\varphi(\mathbf{R}, t) = - \int dt V_0 |\Psi(\mathbf{R} - \mathbf{v}t)|^2 / \hbar \quad (3)$$

is the phase imprinted by the moving Rydberg impurities at a location \mathbf{R} in the BEC. Using the definition of a line integral along the curve $\mathbf{R}' = \mathbf{R} - \mathbf{v}t$, we can rewrite this as

$$\varphi(\mathbf{R}, t) = - \int_{\mathcal{C}} dl V_0 |\Psi[\mathbf{R}'(l)]|^2 / |\mathbf{v}| \hbar, \quad (4)$$

where the curve \mathcal{C} traces the trajectory of the location \mathbf{R} as it moves through the Rydberg electron orbit Ψ in the rest frame of the Rydberg atom. We show Eq. (4) to demonstrate two features. (i) The accumulated phase is a spatial average over $|\Psi|^2$ in the direction of motion. As we will show, this allows impurity tracking with the added practical benefit that oscillatory quantum features in Fig. 1(b) are averaged, so we can replace $V_{gR,n}(\mathbf{R})$ with a smoother classical approximation $V_{c,n}(\mathbf{R})$ as discussed in Sec. IV. This simplification will be used shortly, in Fig. 3. (ii) The phase is proportional to $|\mathbf{v}|^{-1}$ for uniform motion and thus contains velocity information.

¹We neglect the dependence of a_e on electron momentum for simplicity.

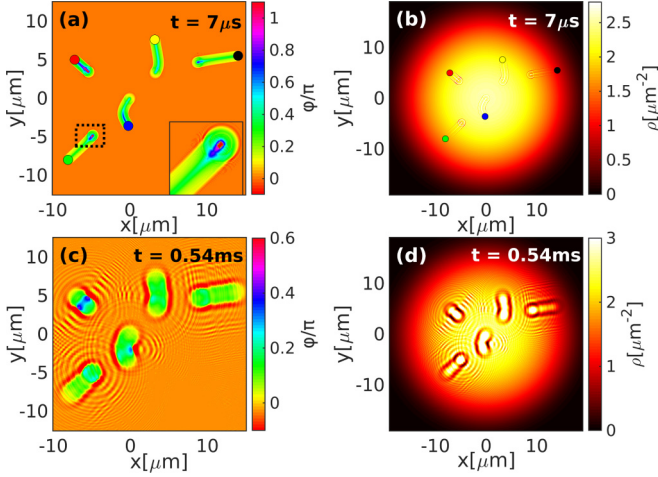


FIG. 3. Tracking Rydberg atoms in a BEC through density or phase information. Five $\nu = 80$ Rydberg excitations are in a ^{87}Rb BEC of $N = 1500$ atoms in a $\omega_r/2\pi = 4$ Hz pancake trap, with transverse strength $\omega_z/2\pi = 1$ kHz. (a) Phase imprinted by Rydberg atoms after $t = \tau_{\text{imp}} = 7 \mu\text{s}$. (b) The density signal at this time is weak. (c) and (d) Assuming impurities are removed at τ_{imp} , the BEC evolution (1) converts the phase signal into clear density signals on the longer timescale $\tau_{\text{mov}} = 0.54$ ms. See also the Supplemental Material [29].

III. PHASE IMPRINTING VERSUS DENSITY MODULATION

Using XMDS [30,31], we have numerically solved the coupled system of the GPE (1) and Newton's equations (2) for a comparatively small 2D BEC cloud, with 3D peak density at the center of $\rho_0 = 4.2 \times 10^{18} \text{ m}^{-3}$. Five atoms are excited to $\nu = 80$ Rydberg states and placed at $t = 0$ initially on the inner starting points of the tracks evident in Fig. 3(a),² which shows the condensate phase $\varphi(\mathbf{R})$. The final position of each atom after an imprinting time $\tau_{\text{imp}} = 7 \mu\text{s}$ is shown by colored circles with size matching the Rydberg electron orbital radius $r_{\text{orb}} = 3a_0\nu^2/2$. Atoms have repelled as in [8], on timescales very short compared to those typical for BECs. While tracks are clearly visible in the condensate phase, the effect on the density in Fig. 3(b) is almost negligible for times as short as τ_{imp} , corresponding to the Raman-Nath regime [32]. The imprinted phase also carries velocity information, since it depends on how long a given location is visited by the impurity as discussed in Sec. II. This is shown in the inset of Fig. 3(a) for the initial atomic acceleration.

Interferometry can deduce a condensate phase pattern [12–16], but is not commonly available. Fortunately, the phase tracks are converted into density tracks through motion of the ground-state atoms. These have received an initial impulse from the passing Rydberg impurity, causing motion on larger timescales $\tau_{\text{mov}} \approx 0.54$ ms in Figs. 3(c) and 3(d). Hence density depressions with 84% contrast appear on either side

²Locations are chosen manually but are consistent with a blockade radius of $r_{\text{bl}} = 6.6 \mu\text{m}$ for excitation Rabi frequency $\Omega = 50/2\pi$ MHz.

of the Rydberg track. These can be read out through *in situ* density measurements [9–11].

Tracking information is dominated by imprinting via the wide tails of the Rydberg electron density, between $x = 10$ and 50 nm in Fig. 1(b). We thus cut off the large central peak at V_{max} as shown in blue, to significantly ease simulations. Tracks were largely independent of this technical step (see Fig. 8).

IV. CLASSICAL ELECTRON DISTRIBUTION

To deal with numerical challenges discussed in Appendix B, for Fig. 3 we have replaced the potential based on the Rydberg electron wave function $V_{gR,n}(\mathbf{R})$ by one based on the corresponding classical probability density (CPD) [33]

$$\rho^{\text{cl}}(\mathbf{R}) = \frac{1}{8\pi^2 R} \frac{1}{\sqrt{\epsilon^2 b^2 - (R - b)^2}}, \quad (5)$$

where $R = |\mathbf{R}|$, $b = -k/2E$ is the semimajor axis for the elliptical electron orbit in a Coulomb field $U(\mathbf{R}) = -k/R$, with E the energy of the ν th level, and $\epsilon = \sqrt{1 + 2EL^2/m_e k^2}$ is the eccentricity. Here L is the angular momentum of the Rydberg state and m_e is the mass of the electron.

Overall we thus employ the classical approximation to the Rydberg-BEC interaction potential given by

$$V_{c,n}(\mathbf{R}) = V_0 \times \begin{cases} \rho^{\text{cl}}(\mathbf{R}), & R < R_{\text{CT}} \\ \rho^{\text{Q}}(\mathbf{R}), & R \geq R_{\text{CT}}, \end{cases} \quad (6)$$

which is sketched in Fig. 1(b) as a red line. In (6), $R_{\text{CT}} = b(1 + \epsilon)$ are the classical turning points.

The two potentials give almost identical results as shown for a Rydberg track in Fig. 4. It is created by a single impurity with velocity $v = 0.7$ m/s traversing a homogeneous 2D condensate ($\rho_{3\text{D}} = 4.2 \times 10^{18} \text{ m}^{-3}$ and $\omega_z/2\pi = 1$ kHz). The difference between phases resulting from $V_{gR,n}(\mathbf{R})$ or $V_{c,n}(\mathbf{R})$ is small [see Fig. 4(b)].

This happens since the motion of the Rydberg impurity causes a local segment of the condensate to experience a spatial average of the electron probability distribution along the direction of motion (see Sec. II). According to the correspondence principle, spatially averaging the oscillatory electron density yields the smooth classical probability distribution [33]. Besides technical utility, this agreement indicates that Rydberg tracking could be used for explorations of the correspondence principle.

V. CONDENSATE HEATING

Experiments report atom loss and heating when sequentially exciting a large number of Rydberg impurities in a BEC [6]. Heating might potentially overwhelm the mechanical effects of Rydberg-BEC interactions that we focus on here. However, we now show that heating is limited in our scenarios, since we consider a substantially smaller number of Rydberg impurities and shorter times.

For this, we use models beyond the mean-field equation (1) using the truncated Wigner approximation (TWA) [34–40]. In brief, this adds quantum fluctuations to the initial state of (1) by the specific addition of random noise. Averaging over an ensemble of solutions, we can then extract the number of uncondensed atoms N_{unc} from the noise statistics as discussed

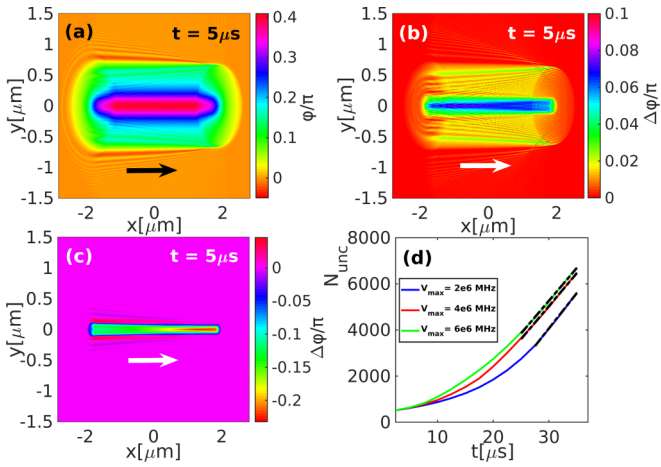


FIG. 4. (a) Condensate phase after motion of a single mobile Rydberg impurity in a homogeneous background using the real potential $V_{gR}(\mathbf{R})$ [thin black line in Fig. 1(b)]. (b) The difference compared to the phases caused by the classical approximation $V_c(\mathbf{R})$ [red line in Fig. 1(b)] is small (see also movie in the Supplemental Material [29]). (c) Modifying the potential cutoff only affects the less relevant central part of the track. We show the difference between phases resulting from $V_{\max} = 2$ and 6 MHz. (d) Number of uncondensed atoms N_{unc} , due to Rydberg impurity determined from the TWA for $V_{\max} = 2, 4$, and 6 MHz (from the bottom line to the top line). Dashed lines match the linear rate equation $dN_{\text{unc}}/dt = \Gamma$, with $\Gamma \approx 280\text{--}300$ atoms / μs . In contrast, for Fig. 3, heating remains negligible.

in Appendix C. We expect the TWA to give reliable results for the short times τ_{imp} considered here [41]. Under the conditions of Fig. 3, we find that up to $\tau_{\text{imp}} = 7 \mu\text{s}$ while Rydberg atoms exist, they cause only eight atoms to become uncondensed. Heating would thus only become significant much later. Thus, in Figs. 4(d) and 5 we rather show the heating for a single impurity with $v = 0.03$ m/s traversing a homogeneous 2D condensate ($\rho_{3D} = 8.5 \times 10^{21} \text{ m}^{-3}$ and $\omega_z/2\pi = 1$ kHz).

The uncondensed atom number $N_{\text{unc}}(t)$ increases with time and then typically shows a linear trend after $t \approx 25 \mu\text{s}$, as shown in Fig. 5(a) for different potential cutoffs V_{\max} at $v = 80$. We also show in Fig. 5(b) that the increase in the cutoff V_{\max} leads to a proportional increase in uncondensed atom number $N_{\text{unc}} \propto V_{\max}$ at a fixed time $N_{\text{unc}}(t_0)$ until this saturates, with mostly unchanged final heating rates.

The linear increase of $N_{\text{unc}}(t)$ at late times in Fig. 5(a) allows the definition of a (final) heating rate Γ via

$$\frac{dN_{\text{unc}}}{dt} = \Gamma, \quad (7)$$

as fitted by dashed lines in Fig. 5(c). We finally show in Fig. 5(d) that asymptotic heating rates Γ scale with the principal quantum number as $\Gamma \sim \nu^{-1}$. For our 2D TWA calculations we employed 256×256 spatial grid points and 129×129 Bogoliubov modes with noise and averaged over 30 000 trajectories. Experiments on heating by mobile Rydberg impurities may unravel incoherent versus coherent aspects of impurity-superfluid interactions, involving critical velocities [42], frictional forces [43], or Cherenkov radiation [44], all due to the creation of elementary excitations [45].

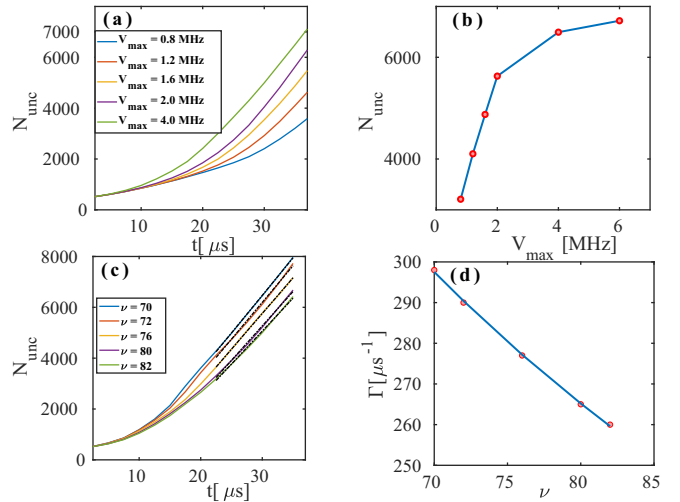


FIG. 5. Incoherent response of host Bose gas to mobile Rydberg impurity. (a) Uncondensed atom number $N_{\text{unc}}(t)$, starting from a vacuum state for different V_{\max} . Here N_{unc} is increasing for larger V_{\max} (from the bottom line to the top line). The initial total number in the simulation box was $N = 70\,000$ atoms. (b) $N_{\text{unc}}(t_0)$ at a fixed time $t_0 = 35 \mu\text{s}$ as a function of V_{\max} , showing saturation. (c) The heating actually decreased for increasing principal quantum number ν (from the top line to the bottom line). (d) Scaling of final heating rate Γ with ν , deduced from linear fits as shown by dashed lines in (c).

VI. DETECTION OF CONDENSATE BACKACTION

We mainly focus on the phase and density tracks imparted by Rydberg impurities on the BEC, however Eq. (1) also includes a backaction of the BEC onto the Rydberg motion: the effective potential in Eq. (2) set by BEC density. This was negligible in Fig. 3 and hence disabled, but can become crucial for denser and smaller condensates (now $N = 28\,000$ atoms with $\omega_r/2\pi = 96$ Hz), shown in Fig. 6. There, just two impurities with $\nu = 80$ are initially separated by $d = 5.57 \mu\text{m}$, symmetrically placed on either side of the center of the condensate, which has a Thomas-Fermi radius

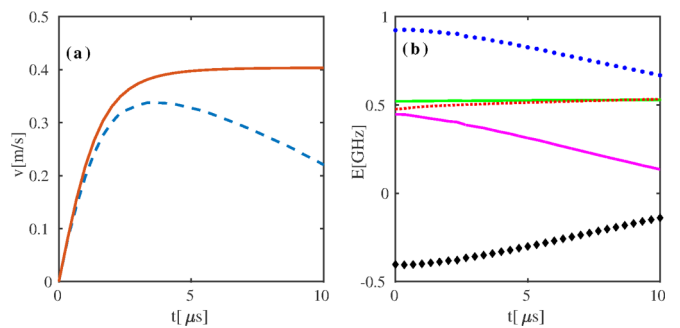


FIG. 6. Backaction of condensate background on dynamic Rydberg atoms. (a) Rydberg velocity as a function of time, with (dashed line) and without (solid line) condensate backaction. (b) Energies with backaction, showing conservation of the total energy E_{tot} (solid green line). Its components are BEC energy (dotted red line), impurity energy (dashed magenta line), and BEC-Rydberg interaction energy E_{int} (black \diamond 's). We also show $E_{\text{tot}} - E_{\text{int}}$ (blue \bullet 's).

$R_{TF} = 8.21 \mu\text{m}$. Rydberg atoms initially accelerate quickly to $v \approx 0.4 \text{ m/s}$ due to vdW repulsion. Once they leave the high-density region of the condensate cloud, the attraction to ground-state atoms provided by the Rydberg electron results in an effective potential well $\tilde{V}(\mathbf{x}_n)$, significantly slowing down the Rydberg impurities as shown in Fig. 6(a).

Had we not included this force in the simulation, the total energy would not be conserved as shown in Fig. 6(b). This total energy of the complete system (Rydberg plus BEC) is given by $E = E_{\text{Ryd}} + E_{\text{BEC}} + E_{\text{int}}$. Here E_{Ryd} is the total energy of the Rydberg impurities

$$E_{\text{Ryd}} = V_{RR}(\mathbf{X}) + \sum_n^{N_{\text{imp}}} \frac{1}{2} m \mathbf{v}_n^2, \quad (8)$$

where \mathbf{v}_n is the velocity of impurity n . The total energy of the BEC is given by the Gross-Pitaevskii energy functional

$$E_{\text{BEC}} = \int d^2\mathbf{R} \phi^*(\mathbf{R}) \left(-\frac{\hbar^2}{2m} \nabla^2 + W(\mathbf{R}) + g_{2D} |\phi(\mathbf{R})|^2 \right) \phi(\mathbf{R}). \quad (9)$$

The interaction energy due to Rydberg-BEC interaction potential V_{gR} is

$$E_{\text{int}} = \sum_n \int d^2\mathbf{R} V_0 |\Psi(\mathbf{R} - \mathbf{x}_n)|^2 |\phi(\mathbf{R})|^2. \quad (10)$$

The backaction effect in Fig. 6 should be observable in experiment, using tracking or conventional techniques.

VII. TRACKING RYDBERG SCATTERING PROCESSES

Our simulation in Fig. 3 demonstrates that kinematic data of mobile Rydberg impurities can be viably extracted through their interaction with a host BEC, mimicking particle physics tracking techniques. Importantly, the required motional time $\tau_{\text{imp}} = 7 \mu\text{s}$ is within the lifetime $\tau \approx 40 \mu\text{s}/N_{\text{imp}} = 8 \mu\text{s}$ of all five atoms expected based on [7] *within the condensate*. However, at $t = 7 \mu\text{s}$ we would already frequently expect to see a Rydberg atom that experienced an inelastic interaction with the BEC, such as a change of the angular momentum state of the atom [7]. Our technique now provides a means of observing such ultracold quantum dynamical processes. We demonstrate the tracking of two of these in Fig. 7. Figure 7(a) shows that terminating tracks allow us to infer the ionization distance d_{ion} of two attractively interacting Rydberg atoms [46–49] even with finite optical resolution. We have assumed an $\mathcal{E} \approx 1 \text{ V/cm}$ extraction field along z such that the ionized electron would leave the BEC within 1 ns. Figure 7(a) also illustrates that the observed pattern could discriminate repulsive and attractive motion even for the same Rydberg states.³ Figure 7(b) shows the track of a single Rydberg atom which experiences an instantaneous angular momentum l -changing collision [7] with a condensate atom at the indicated point. Since the imprinting signature depends on l [25], we can infer the location of the event. Such measurements can then help to

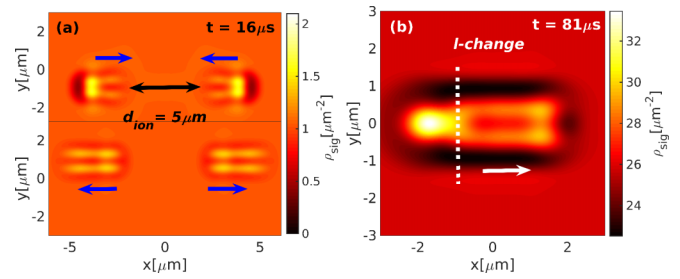


FIG. 7. Condensate tracking of ultracold Rydberg processes (see also [29]). (a) Shown on top is the ionizing attractive collision of Rydberg atoms in states $|v = 80, l = 2, m = 2\rangle$ for quantization along the y axis. We assume instant ionization at $d_{\text{ion}} = 5 \mu\text{m}$ and included $\sigma_{\text{opt}} = 0.5 \mu\text{m}$ optical resolution (see Appendix D). Shown on the bottom are atoms in the same states but moving repulsively. (b) Angular momentum l -changing collision with a background atom from $l = 0$ to $l' = 1$ at the white dashed line, clearly changing the character of the track.

develop theory for Rydberg-Rydberg ionization dynamics or angular momentum evolution in the presence of a continuous measurement, which is not fully established at this stage.

VIII. CONCLUSION

Mobile Rydberg atoms can be tracked through density depressions they cause while passing through a BEC. Modeling this is greatly facilitated by approximating the Rydberg-BEC potential using the classical electron position distribution. On the short timescales required for the tracking, heating and inelastic decay are under control. We demonstrate that BEC-based Rydberg tracking can help advance our understanding of ultracold quantum dynamical processes, such as ionization and state changing collisions. Other effects worthy of exploration may include phonon-mediated Rydberg-Rydberg interactions [50], damping of Rydberg motion [51], and decoherence of multiple excitonic Born-Oppenheimer surfaces [52]. The latter can provide directed energy transport [53,54] or conical intersections [55–57]. Tracking enables detection of such effects and will introduce a well-defined decoherence channel akin to the discussion of [58].

All phenomena discussed here should remain qualitatively unchanged if the direct Rydberg-electron-BEC interaction is replaced with the dressed impurity-BEC long-range interactions discussed in [22]. This turns the range of the imprinting potential and thus the *width* of tracks into a tunable parameter.

ACKNOWLEDGMENTS

We thank Rick Mukherjee and Rejish Nath for fruitful discussions and Arghya Chattopadhyay, Sreeraj Nair, Nilanjan Roy, and Aparna Sreedharan for reading the manuscript. We acknowledge the Science and Engineering Research Board (SERB), Department of Science and Technology (DST), New Delhi, India, for financial support under research Project No. EMR/2016/005462. Financial support from the Max-Planck Society through the MPG-IISER partner group program is also gratefully acknowledged.

³The chosen ones only interact attractively in reality.

APPENDIX A: DIMENSIONALITY REDUCTION FOR GROSS-PITAEVSKII EQUATION

The main article employs a GPE in two spatial dimensions, which eases simulations and in an experiment would ease detection. Let us briefly discuss the approximations that allow the reduction of the 3D GPE to a 2D GPE. The evolution of a BEC in the presence of a Rydberg impurity in 3D is governed by

$$i\hbar \frac{\partial}{\partial t} \phi(\tilde{\mathbf{R}}) = \left(-\frac{\hbar^2}{2m} \nabla_{\tilde{\mathbf{R}}}^2 + W(\tilde{\mathbf{R}}) + g_{3D} |\phi(\tilde{\mathbf{R}})|^2 + \sum_n^{N_{\text{imp}}} V_0 |\Psi(\tilde{\mathbf{R}} - \tilde{\mathbf{x}}_n)|^2 \right) \phi(\tilde{\mathbf{R}}), \quad (\text{A1})$$

where $W(\tilde{\mathbf{R}}) = m[\omega_r^2(x^2 + y^2) + \omega_z^2 z^2]/2$ is the 3D harmonic potential and $\tilde{\mathbf{R}} = [x, y, z]^T$ is the 3D coordinate vector. We take $\omega_z \gg \omega_r$ and assume that the wave function $\phi(\tilde{\mathbf{R}})$ factors into a part for the in-plane coordinate ($\mathbf{R} = [x, y]^T$) and a part for the z direction as $\phi(\tilde{\mathbf{R}}, t) = \phi(\mathbf{R}, t)\phi(z)$. Importantly, $\phi(z)$ is frozen in the harmonic-oscillator ground state along z , normalized to unity. After multiplying by $\phi^*(z)$ and integrating (A1) here along the z direction we obtain Eq. (1), which effectively describes a tightly trapped pancake BEC. We consider parameters for which $\sigma_z = 0.3 \mu\text{m} < r_{\text{orb}} = 0.6 \mu\text{m}$. We can thus assume that the Rydberg wave function does not vary significantly over the range of z with nonvanishing BEC (see Fig. 2). Then, during the 3D to 2D reduction, we can approximate

$$\int dz V_0 |\Psi(\tilde{\mathbf{R}} - \tilde{\mathbf{x}}_n)|^2 |\phi(z)|^2 \approx V_0 |\Psi(\mathbf{R} - \mathbf{x}_n)|^2 \int dz |\phi(z)|^2 = V_0 |\Psi(\mathbf{R} - \mathbf{x}_n)|^2. \quad (\text{A2})$$

Effectively, in Eq. (A2), we thus only use a 2D cut at $z = 0$ through the effective potential $V_{gR,n}(\mathbf{R})$, as shown in Fig. 2.

APPENDIX B: QUANTUM VERSUS CLASSICAL RYDBERG ELECTRON PROBABILITY DISTRIBUTIONS

The Rydberg-condensate interaction potential V_{gR} contains a 2D cut of the quantum probability density (QPD) $\rho^Q(\mathbf{R}) = |\Psi(|\mathbf{R}|)|^2$ (for a single impurity at $\mathbf{x} = 0$). Modeling the ensuing BEC dynamics encounters two major computational challenges. (i) Resolving the highly oscillatory Rydberg wave function in Fig. 1(b) on nanometer scales while spanning the whole host BEC of radius $\sim 20 \mu\text{m}$ necessitates a very large number of discrete spatial points. (ii) At the same time, very short time steps are forced by large interaction energies of the order of 10 GHz between ground-state and Rydberg atoms near the Rydberg core only. We tackle the former point (i) by replacing the QPD in Eq. (1) by the classical probability density (CPD) [33] in Eq. (5).

The CPD becomes ill-defined after the outer classical turning point R_{CT} , where $R_{\text{CT}} = b(1 + \epsilon)$. Therefore, for $R > R_{\text{CT}}$ we revert from (5) to the tail of the QPD for a smooth and well-approximated distribution, as listed in Eq. (6).

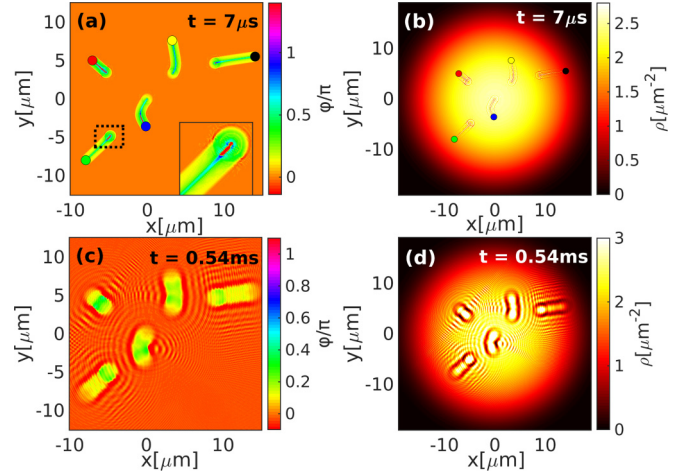


FIG. 8. Same as in Fig. 3 but using the cutoff $V_{\text{max}} = 20$ MHz instead of 2 MHz.

We solve problem (ii) by using a high-energy cutoff at $|V(\mathbf{R})| = V_{\text{max}}$. Due to the minor spatial extent of the potential region affected by the cutoff, its impact on our results is small. This is seen by comparing Fig. 8 with Fig. 3.

APPENDIX C: TRUNCATED WIGNER APPROXIMATION

After its introduction to BECs [34–36] the TWA in a BEC context is described in many articles including the review in [59]. The central ingredient of the method is adding random noise to the initial state of the GPE (1) in order to provide an estimate for the effects of quantum depletion or thermal fluctuations beyond the mean field. We thus use the initial stochastic field

$$\alpha(\mathbf{R}, 0) = \phi_0 + \sum_k [\eta_k u_k(\mathbf{R}) - \eta_k^* v_k^*(\mathbf{R})]/\sqrt{2}, \quad (\text{C1})$$

with random complex Gaussian noises η_k fulfilling $\overline{\eta_k \eta_l} = 0$ and $\overline{\eta_k \eta_l^*} = \delta_{kl}$, where the overbar is a stochastic average. Here $u_k(\mathbf{R})$ and $v_k(\mathbf{R})$ are the usual (2D) Bogoliubov modes in a homogenous BEC with density $\rho = |\phi_0|^2$ [42].

A different symbol $\alpha(\mathbf{R})$ has been chosen for the stochastic field compared to the mean field $\phi(\mathbf{R})$ to emphasize the difference in physical interpretation due to the presence of noise: The stochastic field now allows the approximate extraction of quantum correlations using the prescription

$$\frac{1}{2} [\langle \hat{\Psi}^\dagger(\mathbf{R}') \hat{\Psi}(\mathbf{R}) \rangle + \langle \hat{\Psi}(\mathbf{R}) \hat{\Psi}^\dagger(\mathbf{R}') \rangle] \rightarrow \overline{\alpha^*(\mathbf{R}') \alpha(\mathbf{R})}. \quad (\text{C2})$$

Using restricted basis commutators δ_c [60,61], we can then extract the total atom density

$$n_{\text{tot}}(\mathbf{R}) = \overline{|\alpha(\mathbf{R})|^2} - \frac{\delta_c}{2} \quad (\text{C3})$$

and condensate density $n_{\text{cond}}(\mathbf{R}) = \overline{|\alpha(\mathbf{R})|^2}$ and from these the uncondensed density $n_{\text{unc}}(\mathbf{R}) = n_{\text{tot}}(\mathbf{R}) - n_{\text{cond}}(\mathbf{R})$ (see also [37–39]). Uncondensed atom numbers as a measure of nonequilibrium heating referred to in the main text are finally $N_{\text{unc}} = \int d^2\mathbf{R} n_{\text{unc}}(\mathbf{R})$.

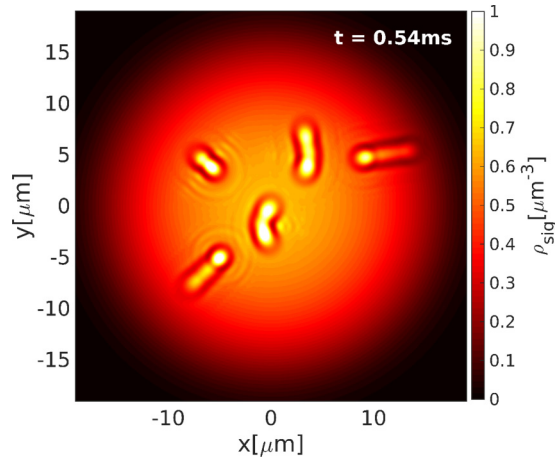


FIG. 9. Same as Fig. 3(d) but assuming an optical resolution $\sigma_{\text{opt}} = 0.5 \mu\text{m}$, as used for Fig. 7.

APPENDIX D: FINITE EXPERIMENTAL RESOLUTION

To assess the feasibility to directly detect features presented here with *in situ* condensate imaging [9–11], we have calculated a density signal at finite resolution $\rho_{\text{sig}}(\mathbf{R})$ by convolution of density data with a Gaussian point spread

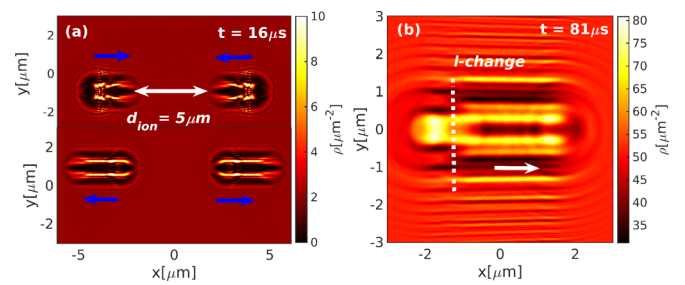


FIG. 10. Same as Fig. 7 but without finite resolution effects.

function

$$\rho_{\text{sig}}(\mathbf{R}) = \mathcal{N} \int d^2\mathbf{R}' e^{-2(|\mathbf{R}-\mathbf{R}'|^2/\sigma_{\text{opt}}^2)} |\phi(\mathbf{R}')|^2, \quad (\text{D1})$$

where σ_{opt} is the optical resolution and \mathcal{N} normalizes the Gaussian to one. Density tracks as shown in Fig. 3 can be seen with $\sigma_{\text{opt}} = 0.5 \mu\text{m}$, challenging but still above the diffraction limit. This is demonstrated in Fig. 9 here. Since the trackable ultracold dynamics processes in Fig. 7 were already shown with finite resolution, we include the raw simulation data in Fig. 10.

-
- [1] D. A. Glaser, *Phys. Rev.* **87**, 665 (1952).
[2] N. N. D. Gupta and S. K. Ghosh, *Rev. Mod. Phys.* **18**, 225 (1946).
[3] K. Kleinknecht, *Phys. Rep.* **84**, 85 (1982).
[4] M. Garcia-Sciveres and N. Wermes, *Rep. Prog. Phys.* **81**, 066101 (2018).
[5] S. Schmid, A. Härter, and J. H. Denschlag, *Phys. Rev. Lett.* **105**, 133202 (2010).
[6] J. B. Balewski, A. T. Krupp, A. Gaj, D. Peter, H. P. Büchler, R. Löw, S. Hofferberth, and T. Pfau, *Nature (London)* **502**, 664 (2013).
[7] M. Schlagmüller, T. C. Liebisch, F. Engel, K. S. Kleinbach, F. Böttcher, U. Hermann, K. M. Westphal, A. Gaj, R. Löw, S. Hofferberth *et al.*, *Phys. Rev. X* **6**, 031020 (2016).
[8] R. C. Teixeira, C. Hermann-Avigliano, T. L. Nguyen, T. Cantat-Moltrecht, J. M. Raimond, S. Haroche, S. Gleyzes, and M. Brune, *Phys. Rev. Lett.* **115**, 013001 (2015).
[9] K. E. Wilson, Z. L. Newman, J. D. Lowney, and B. P. Anderson, *Phys. Rev. A* **91**, 023621 (2015).
[10] T. Gericke, P. Würtz, D. Reitz, T. Langen, and H. Ott, *Nat. Phys.* **4**, 949 (2008).
[11] L. V. Hau, B. D. Busch, C. Liu, Z. Dutton, M. M. Burns, and J. A. Golovchenko, *Phys. Rev. A* **58**, R54 (1998).
[12] J. E. Simsarian, J. Denschlag, M. Edwards, C. W. Clark, L. Deng, E. W. Hagley, K. Helmerson, S. L. Rolston, and W. D. Phillips, *Phys. Rev. Lett.* **85**, 2040 (2000).
[13] A. V. Martin and L. J. Allen, *Phys. Rev. A* **76**, 053606 (2007).
[14] D. Meiser and P. Meystre, *Phys. Rev. A* **72**, 023605 (2005).
[15] R. Gati, B. Hemmerling, J. Fölling, M. Albiez, and M. K. Oberthaler, *Phys. Rev. Lett.* **96**, 130404 (2006).
[16] Y.-J. Wang, D. Z. Anderson, V. M. Bright, E. A. Cornell, Q. Diot, T. Kishimoto, M. Prentiss, R. A. Saravanan, S. R. Segal, and S. Wu, *Phys. Rev. Lett.* **94**, 090405 (2005).
[17] T. F. Gallagher, *Rydberg Atoms* (Cambridge University Press, Cambridge, 1994).
[18] K. Singer, J. Stanojevic, M. Weidemüller, and R. Côté, *J. Phys. B* **38**, S295 (2005).
[19] S. Weber, C. Tresp, H. Menke, A. Urvoy, O. Firstenberg, H. P. Büchler, and S. Hofferberth, *J. Phys. B* **50**, 133001 (2017).
[20] T. Niederprüm, O. Thomas, T. Manthey, T. M. Weber, and H. Ott, *Phys. Rev. Lett.* **115**, 013003 (2015).
[21] G. E. Astrakharchik and L. P. Pitaevskii, *Phys. Rev. A* **70**, 013608 (2004).
[22] R. Mukherjee, C. Ates, W. Li, and S. Wüster, *Phys. Rev. Lett.* **115**, 040401 (2015).
[23] V. Shukla, R. Pandit, and M. Brachet, *Phys. Rev. A* **97**, 013627 (2018).
[24] S. Middelkamp, I. Lesanovsky, and P. Schmelcher, *Phys. Rev. A* **76**, 022507 (2007).
[25] T. Karpiuk, M. Brewczyk, K. Rażewski, A. Gaj, J. B. Balewski, A. T. Krupp, M. Schlagmüller, R. Löw, S. Hofferberth, and T. Pfau, *New J. Phys.* **17**, 053046 (2015).
[26] G. Verma, U. D. Rapol, and R. Nath, *Phys. Rev. A* **95**, 043618 (2017).
[27] C. H. Greene, A. S. Dickinson, and H. R. Sadeghpour, *Phys. Rev. Lett.* **85**, 2458 (2000).
[28] Ł. Dobrek, M. Gajda, M. Lewenstein, K. Sengstock, G. Birkl, and W. Ertmer, *Phys. Rev. A* **60**, R3381(R) (1999).
[29] See Supplemental Material at <http://link.aps.org/supplemental/10.1103/PhysRevA.99.043616> for a movie.

- [30] G. R. Dennis, J. J. Hope, and M. T. Johnsson, XMDS2, <http://www.xmnds.org/>
- [31] G. R. Dennis, J. J. Hope, and M. T. Johnsson, *Comput. Phys. Commun.* **184**, 201 (2013).
- [32] H. Müller, S.-w. Chiow, and S. Chu, *Phys. Rev. A* **77**, 023609 (2008).
- [33] A. Martín-Ruiz, J. Bernal, A. Frank, and A. Carbajal-Dominguez, *J. Mod. Phys.* **4**, 818 (2013).
- [34] M. J. Steel, M. K. Olsen, L. I. Plimak, P. D. Drummond, S. M. Tan, M. J. Collett, D. F. Walls, and R. Graham, *Phys. Rev. A* **58**, 4824 (1998).
- [35] A. Sinatra, C. Lobo, and Y. Castin, *Phys. Rev. Lett.* **87**, 210404 (2001).
- [36] A. Sinatra, C. Lobo, and Y. Castin, *J. Phys. B* **35**, 3599 (2002).
- [37] S. Wüster, B. J. Dąbrowska-Wüster, A. S. Bradley, M. J. Davis, P. B. Blakie, J. J. Hope, and C. M. Savage, *Phys. Rev. A* **75**, 043611 (2007).
- [38] S. Wüster, B. J. Dąbrowska-Wüster, S. M. Scott, J. D. Close, and C. M. Savage, *Phys. Rev. A* **77**, 023619 (2008).
- [39] B. J. Dąbrowska-Wüster, S. Wüster, and M. J. Davis, *New J. Phys.* **11**, 053017 (2009).
- [40] A. A. Norrie, R. J. Ballagh, C. W. Gardiner, and A. S. Bradley, *Phys. Rev. A* **73**, 043618 (2006).
- [41] A. Polkovnikov, *Phys. Rev. A* **68**, 053604 (2003).
- [42] C. J. Pethik and H. Smith, *Bose-Einstein Condensation in Dilute Gases* (Cambridge University Press, Cambridge, 2002).
- [43] A. G. Sykes, M. J. Davis, and D. C. Roberts, *Phys. Rev. Lett.* **103**, 085302 (2009).
- [44] I. Carusotto, S. X. Hu, L. A. Collins, and A. Smerzi, *Phys. Rev. Lett.* **97**, 260403 (2006).
- [45] J. Suzuki, *Physica A* **397**, 40 (2014).
- [46] W. Li, P. J. Tanner, and T. F. Gallagher, *Phys. Rev. Lett.* **94**, 173001 (2005).
- [47] T. Amthor, M. Reetz-Lamour, S. Westermann, J. Denskat, and M. Weidemüller, *Phys. Rev. Lett.* **98**, 023004 (2007).
- [48] M. Viteau, A. Chotia, D. Comparat, D. A. Tate, T. F. Gallagher, and P. Pillet, *Phys. Rev. A* **78**, 040704(R) (2008).
- [49] H. Park, E. S. Shuman, and T. F. Gallagher, *Phys. Rev. A* **84**, 052708 (2011).
- [50] J. Wang, M. Gacesa, and R. Côté, *Phys. Rev. Lett.* **114**, 243003 (2015).
- [51] P. Ostmann and W. T. Strunz, [arXiv:1707.05257](https://arxiv.org/abs/1707.05257).
- [52] S. Wüster and J. M. Rost, *J. Phys. B* **51**, 032001 (2018).
- [53] S. Wüster, C. Ates, A. Eisfeld, and J. M. Rost, *Phys. Rev. Lett.* **105**, 053004 (2010).
- [54] S. Möbius, S. Wüster, C. Ates, A. Eisfeld, and J. M. Rost, *J. Phys. B* **44**, 184011 (2011).
- [55] S. Wüster, A. Eisfeld, and J. M. Rost, *Phys. Rev. Lett.* **106**, 153002 (2011).
- [56] K. Leonhardt, S. Wüster, and J. M. Rost, *Phys. Rev. Lett.* **113**, 223001 (2014).
- [57] K. Leonhardt, S. Wüster, and J. M. Rost, *J. Phys. B* **50**, 054001 (2017).
- [58] S. Wüster, *Phys. Rev. Lett.* **119**, 013001 (2017).
- [59] P. Blakie, A. Bradley, M. Davis, R. Ballagh, and C. Gardiner, *Adv. Phys.* **57**, 363 (2008).
- [60] A. A. Norrie, R. J. Ballagh, and C. W. Gardiner, *Phys. Rev. A* **73**, 043617 (2006).
- [61] A. A. Norrie, Ph.D. thesis, University of Otago, 2005, available at <http://www.physics.otago.ac.nz/nx/jdc/jdc-thesis-page.html>